JOURNAL OF AIRCRAFT
Vol. 41, No. 3, May–June 2004

Transonic Unsteady Aerodynamics of the F/A-18E Under Conditions Promoting Abrupt Wing Stall

David M. Schuster*
NASA Langley Research Center, Hampton, Virginia 23681-2199
and
James E. Byrd†
Lockheed Martin Engineering and Sciences, Hampton, Virginia 23681-2199

A transonic wind-tunnel test of an 8% F/A-18E model was conducted in the NASA Langley Research Center 16-Foot Transonic Tunnel to investigate the abrupt wing stall characteristics of this aircraft. During this test, both steady and unsteady measurements of balance loads, wing surface pressures, wing-root bending moments, and outer-wing accelerations were performed. The test was conducted with a wide range of model configurations and test conditions in an attempt to reproduce behavior indicative of the abrupt wing stall phenomenon experienced in full-scale aircraft during flight tests. This study focuses on the analysis of the unsteady data acquired during this test. Though the test apparatus was designed to be effectively rigid, model motions due to sting and balance flexibility were observed during the testing, particularly when the tunnel was operated under conditions representative of those where wing drop was experienced in flight. The correlation between observed aerodynamic frequencies and model structural frequencies is analyzed and presented. Significant shock motion and separated flow are observed as the aircraft pitches through the abrupt wing stall region. A shock-tracking strategy has been formulated to observe this phenomenon. Using this technique, the range of shock motion as the aircraft encounters abrupt wing stall conditions is readily determined. Spectral analysis of the shock motion shows the frequencies at which the shock oscillates in the abrupt wing stall region, and probability density function analysis of the shock location shows the propensity of the shock to take on a bistable and even tristable character in the abrupt wing stall flight regime.

Nomenclature

C_p	=	pressure coefficient
$C_{p\text{Shock}}$	=	pressure coefficient representing center of a shock wave
M	=	Mach number
X/C	=	fraction of local wing chord
X/C_{Shock}	=	chordwise location of a shock wave in fraction of local chord
α	=	angle of attack
σ	=	standard deviation

Introduction

IN the mid-1990s, F/A-18E/F aircraft undergoing preproduction flight testing encountered a lateral instability, characterized as wing drop, when performing some high-speed, high-load-factor turning maneuvers.[1] This instability was ultimately traced to abrupt wing stall (AWS) of either the left or right wing, causing a sudden and severe roll-off in the direction of the stalled panel. An important distinction between wing drop and AWS is that wing drop is the dynamic response of an aircraft to an aerodynamic event, whereas AWS is an aerodynamic event that can trigger wing drop.

Further magnifying the importance of this aerodynamic phenomenon is the fact that a large number of jet-age fighter aircraft have encountered wing rock and/or wing drop instabilities.[2] Unfortunately, these lateral problems were not adequately predicted by developmental ground-based testing before actual aircraft flight tests. In some cases, modifying the geometry of the aircraft, such as rescheduling leading- or trailing-edge flap deflections, or adjusting flight control laws could mitigate these instabilities. In other cases, the aircraft's operational envelope was such that the adverse behavior was rarely encountered in operational service and was deemed acceptable. Unfortunately, in the case of the preproduction versions of the F/A-18E/F, the motions were relatively severe. Changes in the wing leading- and trailing-edge flap scheduling were effective in reducing the severity of the problem but could not completely eliminate the wing drop. Because the instability appeared in a critical portion of the flight envelope, modification of operational parameters was infeasible.

After significant expenditure of flight test and analysis resources, the lateral activity was mitigated by two modifications. First, the wing leading-edge flap deflection with Mach number and angle of attack was increased, resulting in an "80% solution".[1] However, even with the revised flap schedule the aircraft exhibited undesirable lateral activity. The second critical modification involved replacing the solid-door wing-fold fairing with a porous door. Together, these modifications ultimately solved the wing-drop problem on the F/A-18E/F. Though these flight-derived fixes for the F/A-18E/F solved its handling problems, the fact remains that this instability was not predicted or anticipated prior to flight test. Given the susceptibility of modern fighter aircraft to encountering uncontrolled lateral dynamics and the near-catastrophic technical and political consequences of this type of instability for the future of the F/A-18E/F program, a cooperative NASA/Navy/Air Force research effort to investigate, understand, predict, and avoid AWS in future aircraft programs has been devised and executed.[3]

A key component of this research is the development of an experimental program to investigate the AWS phenomenon and devise a strategy for future testing of aircraft susceptible to AWS. One of the experimental strategies employed in this investigation focused on implementing and enhancing standard static wind-tunnel test techniques that might be applied during routine aircraft development.

Presented as Paper 2003-0593 at the 41st Aerospace Sciences Meeting and Exhibit, Reno, NV, 6 January 2003; received 1 August 2003; revision received 31 October 2003; accepted for publication 1 November 2003.

*Senior Research Engineer, Aeroelasticity Branch, MS 340; david.m.schuster@nasa.gov. Associate Fellow AIAA.
†Staff Aeronautical Engineer, MS 280; j.e.byrd@larc.nasa.gov.

Because AWS and the resulting lateral instabilities are dynamic or, at best, highly sensitive quasi-static phenomena, measurement of unsteady wing-surface pressures, loads, and accelerations were incorporated into the test procedures to investigate potential unsteady causes and/or indicators of AWS.

This paper describes the wind-tunnel model employed, unsteady instrumentation, associated data-acquisition techniques, summary analysis results, and their implications for the prediction and detection of the AWS phenomenon. In addition, the structural characteristics of the experimental setup were assessed and compared with the aerodynamic loads to determine whether the structural flexibility of the experimental hardware made a significant contribution to the observed unsteady aerodynamics.

Wind-Tunnel Model, Instrumentation Layout, and Data Acquisition

The model tested in the NASA Langley Research Center (LaRC) 16-Foot Transonic Tunnel (16-Ft TT) is a stainless-steel 8% model of the F/A-18E. The model is the primary aerodynamic performance article used in the development of this aircraft. Because the objectives of this test involved significant enhancement of the basic instrumentation package present on the baseline model, new wings were fabricated containing a combination of steady-pressure ports, in situ unsteady-pressure transducers, outer-wing accelerometers, and wing-root-bending strain gauges. A six-component internal balance rounds out the primary instrumentation package for the model. A photograph of the model installed in the 16-Ft TT is shown in Fig. 1, and a more comprehensive description of the model and test procedures is available in Ref. 4.

Several variations of wing leading- and trailing-edge flap deflection were tested and evaluated. In the F/A-18E/F development program, the 80% solution utilized the 6.1.3 version of the flight control laws and was represented during wind-tunnel testing with a 10/10/5-deg flap set, where the deflections correspond to the leading-edge flap deflection, the trailing-edge flap deflection, and the aileron deflection, respectively. In this paper, this 10/10/5-deg wing flap set on the baseline aircraft will be emphasized. The porous-door fix implemented for the production aircraft is not included in the test data presented here. Testing was performed under atmospheric conditions over a range of Mach numbers, but the bulk of testing occurred at Mach 0.8 and 0.9. Data at Mach 0.9 are the focus of this paper. Similar aerodynamic characteristics were observed at Mach 0.8.

This Mach number and flap setting are representative of conditions under which wing drop was experienced during flight test. At this Mach number, AWS is observed at angles of attack between 9 and 10 deg, and hereafter this will be referred to as the AWS angle-of-attack regime or range.

Identical steady-pressure instrumentation sets were included on both the left and right wings, but because of limitations of dynamic data acquisition and the cost and complexity of including unsteady-pressure instrumentation in a model of this type, only the left wing included unsteady-pressure measurements. The layout of the instrumentation package on the upper surface of this wing panel is shown in Fig. 2.

Fig. 1 F/A-18E model installed in LaRC 16-Ft TT.

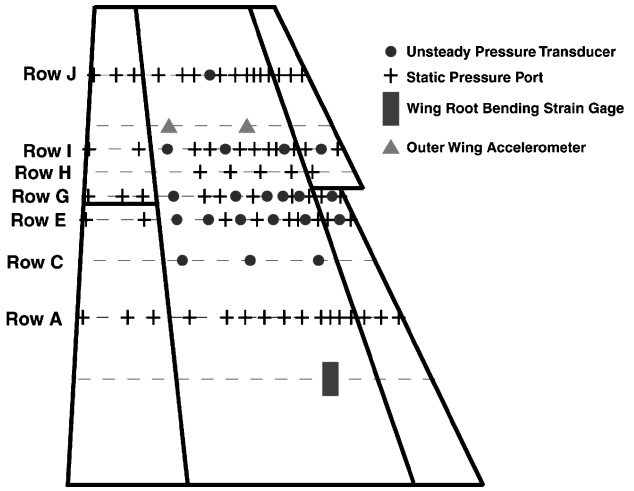

Fig. 2 Instrumentation layout for the left-wing upper surface.

In all, the model instrumentation consisted of 23 unsteady-pressure transducers, four outer-wing accelerometers, and two wing-bending strain gauges on which time-synchronized data were acquired. Of the 23 unsteady-pressure transducers, 20 were located on the upper surface of the left wing. The remaining three transducers were located on the lower surface of the left wing. Both the left and right wings were instrumented with outer-wing accelerometers (two each) and wing-root bending gauges (one each). The dynamic-data-acquisition system employed in this test was capable of acquiring time-synchronized data on 32 channels, and so three balance channels were also dynamically sampled. The three balance channels chosen for dynamic sampling were the axial force, pitching moment, and rolling moment components.

During the test, the unsteady data were acquired in 10-s records on magnetic tape, using VHS videocassettes, and digitized posttest. In the digitizing process the data were sampled at a rate of 1000 samples per second for 10 s. A 200-Hz antialiasing filter was applied to the data during the digitization process. The range of the pressure gauges is ± 15 psi (103.4 kPa). The resolution of the pressure gauges is 0.00125 psi/bit (0.00862 kPa/bit). Under typical flow conditions in the wind tunnel this produces a pressure-coefficient resolution of 0.00023/bit. The resolution of the accelerometers is 0.00625 g/bit. Time-history records and mean, standard deviation, and maximum and minimum values were processed for each data point and channel in the data set. The data were stored on a set of compact disks for further data processing by the AWS team.

Dynamic Data Analysis

In addition to simply trying to gain a physical understanding of the unsteady flow on the aircraft under AWS conditions, the analysis of the dynamic data was driven by a number of factors including wind-tunnel model vibration. Under test conditions where AWS had been encountered in flight, the model became quite active on the balance/sting support system, exhibiting noticeable pitch, plunge, and roll vibrations. Similar balance/sting dynamics, though at somewhat higher angles of attack, are described by Mabey et al.[5] In addition, dynamic loads monitored by the balance dynamics display unit indicated that the model was experiencing high axial-force loads that were near to and occasionally in excess of the prescribed balance limits. On several occasions, balance fouling was detected due to these oscillations. Therefore, a primary objective of the unsteady-data analysis was to determine whether the structural vibrations observed in the tunnel were simply a response to the extreme unsteady aerodynamics experienced under the AWS conditions, or whether there was indeed an aeroelastic coupling whereby the structural

Table 1 Modes and associated frequencies obtained from posttest GVT

Mode	Frequency, Hz
Sting yaw	6.86
Sting vertical	11.69
Coupled sting/balance	13.06
Yaw	
Balance yaw	18.71
Balance pitch	20.21
Balance roll	22.77
Antisymmetric wing-bending	77.3
Balance axial	97.8

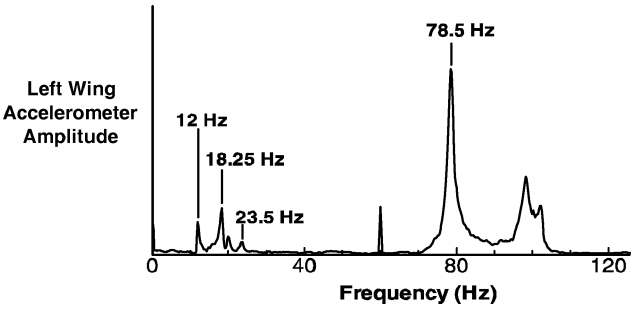

a) Right wing tip rap

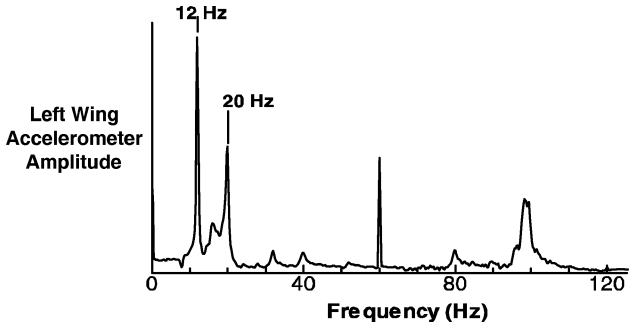

b) Forward fuselage rap

Fig. 3 Frequency response of a left-wing accelerometer to right-wing and forward-fuselage raps.

oscillations had a significant, discernible impact on the unsteady aerodynamics.

To aid in this portion of the analysis, structural-dynamic properties of the model, balance, and sting mounted in the 16-Ft TT were measured through simple "rap" tests of the model between test runs and a more detailed ground-vibration test (GVT) of the model posttest. The rap tests were conducted by simply hitting the model with a closed fist on the nose and wing tip of the aircraft and recording vibration-time-history data using the balance channels, outer-wing accelerometers, and wing-root-bending strain gauges. A signal analyzer was used to process these time-history data and produce frequency responses. Sample results of two of these tests are shown in Fig. 3.

In Fig. 3, several frequency peaks are labeled, which correspond to dominant structural modes of the model/balance/sting system. The peak observed at 60 Hz is due to electrical interference. Hitting the forward fuselage tends to excite longitudinal structural modes such as sting and balance pitch, whereas hitting the wing tip excites lateral structural modes such as roll and antisymmetric wing-bending. Using visual observation and experience, structural modes such as sting pitch, balance pitch, and balance roll could be matched up with observed frequencies. The posttest GVT corroborated these results by quantitatively matching the frequencies observed in the rap tests to the structural motions. Results from this GVT are presented in Table 1. Of the modes listed, sting vertical, balance pitch, balance roll, and antisymmetric wing bending modes were most often observed on the wing accelerometers and strain gauges during periods of high model excitation in the AWS flight regime.

Unsteady readings from the balance, accelerometers, and strain gauges were dominated by the structural frequencies of vibration, and independent unsteady aerodynamic traits were difficult to separate from the measurements on these instruments. Thus, the unsteady-pressure measurements became the primary source of information concerning the unsteady aerodynamics present on the vehicle in the AWS flight regime.

Several methods were employed to analyze and reduce the unsteady-pressure data, ranging from investigation of the raw pressure time histories on individual transducers to the identification and tracking of flow structures such as shock waves. Pressure distributions acquired on the baseline F/A-18E with the 10/10/5-deg flap set at Mach 0.9 are used in the following unsteady-pressure data analyses. Pressures along row E of Fig. 2 are the primary focus of this analysis because this is the row most highly populated with unsteady transducers. It is also in close proximity to the leading-edge snag, which has been identified as a key region of interest in the investigation of AWS on the F/A-18E/F.[4,6,7] It is important to note, however, that the flowfield under these conditions is highly three dimensional, and the spanwise unsteadiness of the shocks and separated regions is also important to understanding the flow on this wing.

Figure 4 shows pressure-coefficient time-history data acquired at a single pressure transducer in row E near the center of the wing box at Mach 0.9. The location of this transducer is circled on the image of the planform at the bottom of the figure. Time histories are plotted in 1-deg angle-of-attack increments from 6.5 to 9.5 deg. The pressure coefficient plotted is the complete pressure coefficient,

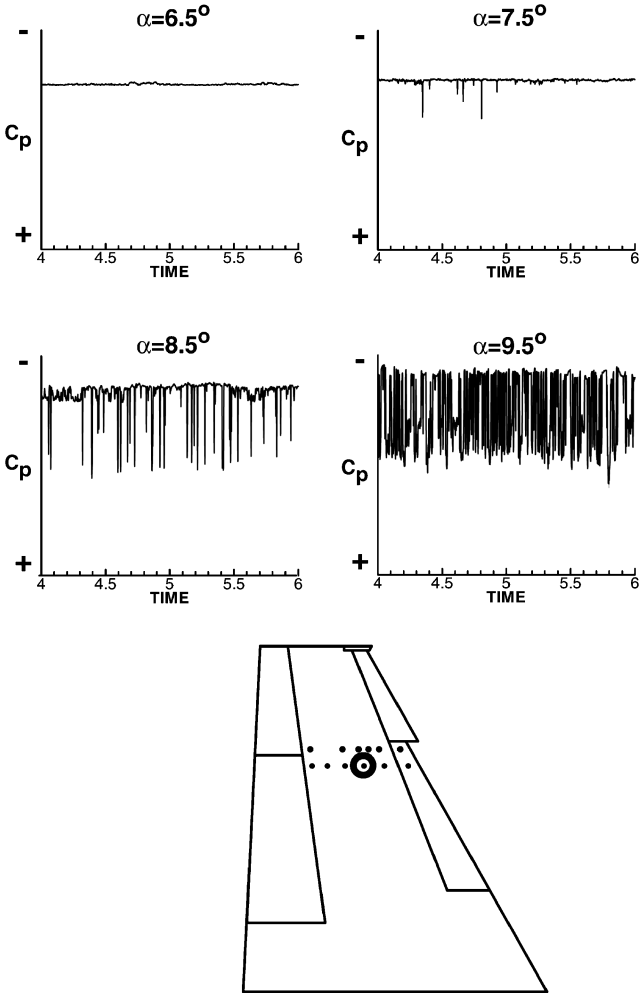

Fig. 4 Pressure-coefficient time history at a single point on the wing for a series of angles of attack; $M = 0.90$.

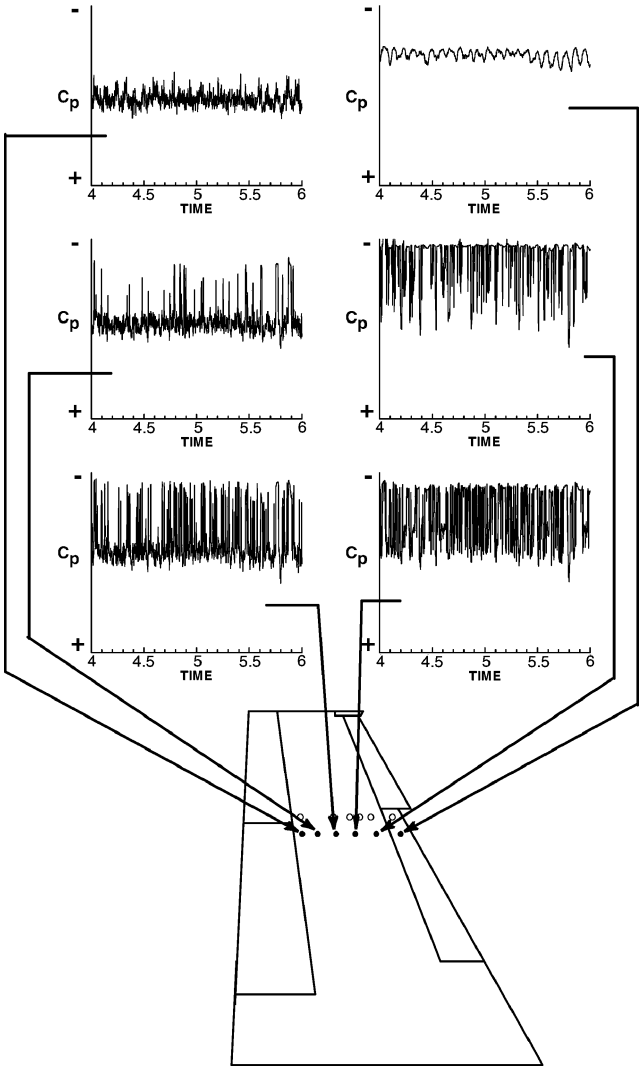

Fig. 5 Pressure-coefficient time histories at a constant spanwise station; $M = 0.90$, $\alpha = 9.5$ deg.

as opposed to just the fluctuating component of the pressure. The vertical scale in all of the plots is identical and is also the same scale as used on subsequent plots.

Figure 4 clearly shows the progression of the shock wave forward on the wing as the angle of attack is increased into the AWS region. At 6.5 deg, the pressures measured by the transducer are very stable and constant across the time record. At 7.5 deg, the first hint of a shock moving onto this chordwise location is seen in the discrete spikes in the pressure time history. By 8.5 deg, the spikes are much more prevalent, and finally at 9.5 deg the time history is saturated with pressure spikes as the shock moves back and forth across the pressure transducer. Hwang and Pi[8] observed a similar unsteady-pressure character in their buffet and wing-rock analysis of the F-5A aircraft.

Figure 5 shows a similar pressure time-history plot, but in this case the angle of attack is fixed at 9.5 deg and the series of plots represents the time histories for the entire chordwise row of transducers. There are several interesting features observed in this figure. First, the difference between a separated-flow unsteady-pressure signature and the pressure signature generated by a shock passage can be seen by looking at the aftmost transducer and the four transducers in front of it. The flow separates just in front of the trailing-edge flap, and the aftmost transducer shows the pressure signature for this type of flow. The transducers immediately forward of this location show the spiky nature of the pressures as shocks pass over the transducer. In addition, the amplitude of the pressure variation is considerably smaller for the separated-flow case as compared to the shock-passage case. The root-mean-square (rms) value of the fluctuating pressure coefficient is approximately 0.05 on the aftmost transducer, whereas it is in the range of 0.15–0.20 on the four forward transducers. These fluctuating pressure levels and associated flow characteristics are consistent with those quoted by Mabey in Ref. 9.

The second feature to recognize in Fig. 5 is that the shock is moving over the entire length of the center wing box under these conditions. Animation of the unsteady-pressure distribution along this row confirms this extreme degree of shock motion. Finally, the structural vibration of the model on the sting/balance system shows up on the forwardmost pressure transducer. The pressure at this location of the wing is very sensitive to angle of attack, and as the model pitches and plunges on the balance/sting support system, the pressure transducer senses the oscillation. A frequency analysis of the pressure time history at this transducer shows a peak at approximately 12 Hz, which, per Table 1, coincides with the sting vertical-bending structural mode.

Figure 6 illustrates one of the cases where a bistable character was observed in the pressure data. This figure shows the measured pressure time histories near the leading edge of the wing at 6.5, 7.0, and 7.5-deg angles of attack. At 6.5 and 7.5 deg, the pressure traces are stable and virtually constant but at significantly different pressure levels. The rms value of the fluctuating pressure coefficient is on the order of 0.008 for both of these angles of attack, which, by Mabey's[9] criteria, is typical for an attached boundary-layer flow. At 7.0 deg the pressure tends to snap back and forth between the two pressure levels. The rms fluctuating pressure coefficient at this angle jumps to 0.11, which is indicative of a separation-reattachment point. In addition, in the early part of the 7.0-deg time history, the pressure

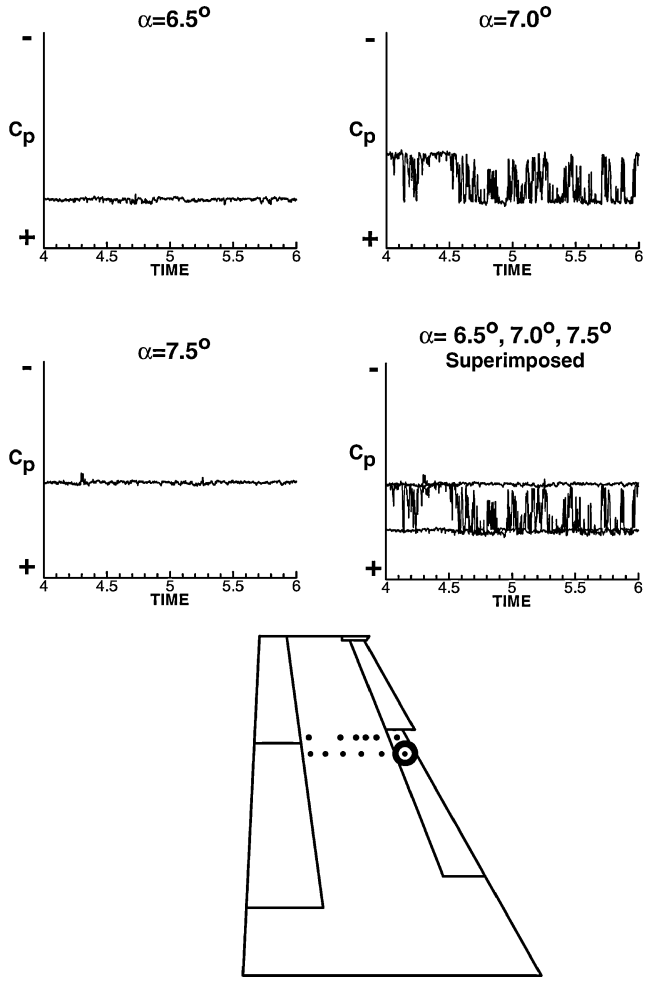

Fig. 6 Pressure-coefficient time histories near the wing leading edge for a series of angles of attack; $M = 0.90$.

seems to be based at the 6.5-deg angle-of-attack level and spikes down to the 7.5-deg level. At about 4.6 s, the character of the time history changes and tends to be based at the 7.5-deg level of pressure spiking up to the 6.5-deg level. To further illustrate how tightly the 7.0-deg fluctuations are bounded by the pressures at 6.5 and 7.5 deg, a fourth plot superimposing the time histories at the three angles of attack is included in the lower-right-hand corner. Preliminary analysis suggests that this is a leading-edge vortex rolling up over the pressure transducer, but computational fluid dynamics, pressure-sensitive paint, and oil-flow images have not been able to confirm this assessment.

Channel statistics were compiled for each unsteady measurement acquired in the test. These statistics included the mean value and standard deviation for each time history, as well as the maximum and minimum values. The mean and standard deviation for the complete sample were computed before the maximum and minimum values were searched for. Given this information, any individual pressure that fell outside a 3σ band about the computed mean was excluded from consideration for the maximum or minimum pressure value because it is statistically insignificant. Plotted as standard pressure coefficient vs fraction of wing chord, these statistics provide further insight into the structure and unsteadiness of the flowfield at AWS conditions.

Figure 7 plots the mean, maximum, and minimum pressures as a fraction of chord for the row E transducers at Mach 0.9 at nominal angles of attack of 4, 7.5, and 9.5 deg. In these plots, the mean pressures are a combination of data from the steady-pressure ports and the unsteady-pressure transducers. Mean pressure values that do not have accompanying maximum and minimum triangles represent pressures acquired on the steady ports. At 4-deg angle of attack a shock is located on the wing in the vicinity of 65% chord, and the flow is very steady forward of the shock, as evidenced by the close proximity of the maximum and minimum pressure values to their corresponding mean pressures. At 7.5-deg angle of attack, the mean location of the shock has moved forward to the vicinity of 40% chord, and there is significant unsteadiness in the pressures in the vicinity of the shock. This angle of attack is approaching, but still well below, the AWS angle-of-attack range. At 9.5-deg angle of attack, the mean pressures show no discernible shock but rather a smooth recompression from 16% to 50% chord. The unsteadiness is severe under these conditions with large differences in the maximum and minimum pressure at each measurement location between 18% and 44% chord. The smooth nature of the mean pressure in this region is misleading and is due to the high degree of unsteadiness in the pressure distribution at this condition, which is in the heart of the AWS region for this Mach number and flap setting.

Figure 8 further illustrates the true nature of the pressure distribution at 9.5-deg angle of attack. Here the instantaneous pressures at two instants in the 10-s record are superimposed on the mean, maximum, and minimum pressures plotted in the preceding figure. In Fig. 8a, there is a shock in the vicinity of 25% chord, whereas 0.4 s later, shown in Fig. 8b, the shock is in the vicinity of 40% chord. Animation of the instantaneous pressures clearly shows the shock moving back and forth between these two positions. However, these animations also show that the pressure distribution will momentarily stabilize in one or more configurations. Therefore, the shock motion cannot always be characterized as oscillatory and it sometimes snaps between discrete states. Although it is difficult to relate this phenomenon to a specific geometric characteristic of the wing, there are two characteristics that strongly influence the unsteady flow at this location. The first is the leading-edge snag, which tends to generate a highly three-dimensional unsteady separated flow in this vicinity. The second is the relatively flat geometry of the wing upper surface, which allows the shock to move large distances over the wing surface with small changes in flow parameters. This behavior is an important feature of the flow and may be a significant contributor to and/or trigger for the AWS and wing-drop phenomena.

In the AWS region, the shock formation and motion is a dominant feature of the unsteady-flowfield. At angles of attack below the AWS region there is minimal unsteadiness in the flow. At angles of attack above the AWS region, the flow is massively separated, and although it is unsteady, the magnitude of the pressure fluctuation is significantly smaller than in the AWS region. To further quantify the nature of the shock and its motion in the AWS region, a simple-shock tracking method has been developed, as shown in Fig. 9. For a given configuration at a given Mach number and angle of attack, a pressure representing the center of the shock is chosen, as designated by $C_{p_{\text{Shock}}}$ in the figure. At each point in the pressure time-history

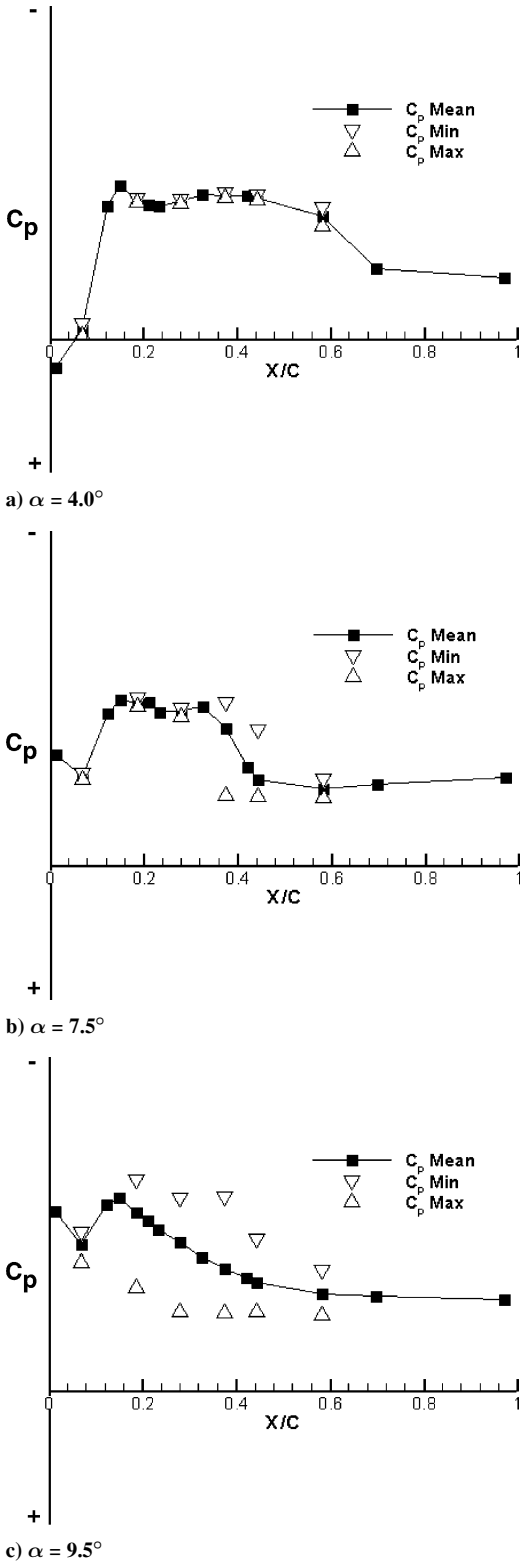

a) α = 4.0°

b) α = 7.5°

c) α = 9.5°

Fig. 7 Row E mean, maximum, and minimum pressure distributions at three angles of attack; M = 0.90.

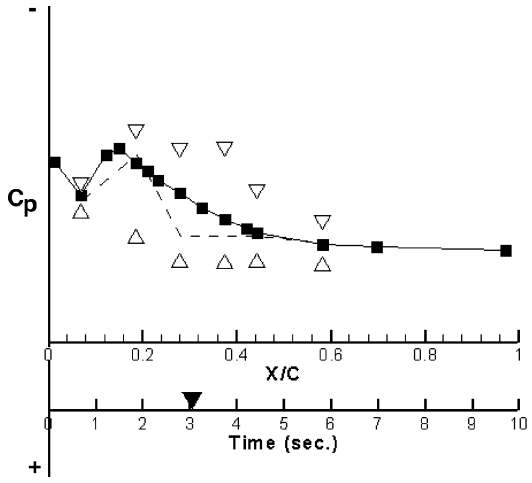

a) Time = 3.0 sec

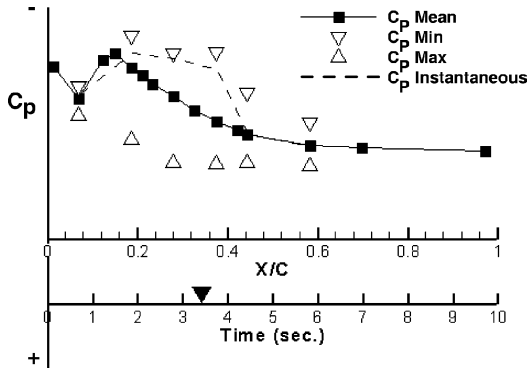

b) Time = 3.4 sec

Fig. 8 E-row pressure distributions including instantaneous pressures at two different times; $M = 0.90$, $\alpha = 9.5$ deg.

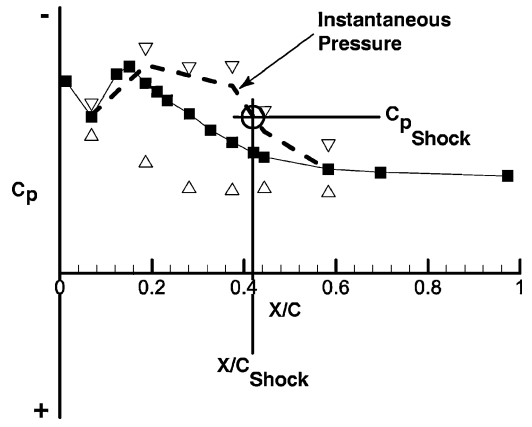

Fig. 9 Strategy implemented for tracking shock motion.

record, the approximate shock location is determined by linearly interpolating for the location (X/C_{Shock}) where the instantaneous pressure distribution crosses the chosen pressure-coefficient level. This effectively provides a time history of the shock location, which can be further processed.

This method has been used in this study to support two principal conclusions. The first is that there are unsteady motions of dominant flow features, namely shock waves, which do not correlate with the structural motion of the vehicle. In other words, the unsteady aerodynamics experienced on the F/A-18E model under AWS conditions are not a direct result of the structural vibrations encountered due to the balance/sting support system. This conclusion is borne out in Figs. 10 and 11, which compare the frequency response of the shock location for the row E pressures with the frequency response for the

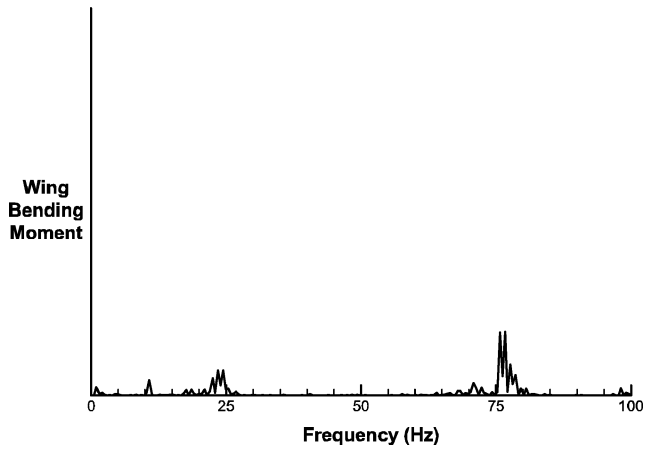

a) Structural dynamics

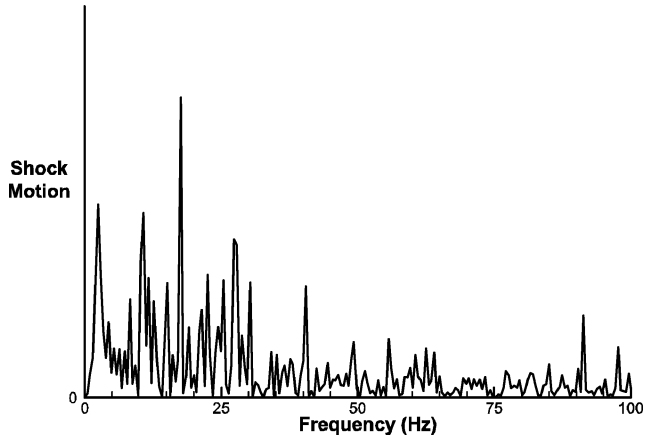

b) Unsteady aerodynamics

Fig. 10 Comparison of model structural dynamic and unsteady aerodynamic frequency content; $M = 0.90$, $\alpha = 6.5$ deg.

wing-root-bending strain gauge. The shock location data represent the primary unsteady aerodynamic forcing function applied to the system, and the strain-gauge data represent the structural response of the system. Figure 10 makes the comparison at Mach 0.9 and 6.5-deg angle of attack, which is below the AWS angle-of-attack region of interest. Figure 11 makes the same comparison with the same plotting scale factors at 9.5-deg angle of attack, where the aircraft is in the middle of the AWS angle-of-attack range.

The first thing to note is the significant difference in the magnitude of structural response between the two angles of attack. At 6.5 deg, the strain-gauge data have much lower amplitude with a frequency content similar to that of the 9.5-deg angle-of-attack case. The frequency response of the strain gauge is characterized as relatively discrete peaks at frequencies that can be correlated with those of Table 1. In contrast, the shock motion in both figures is characterized by a large number of peaks of similar amplitude over a relatively broad band of frequencies. More important, there are no particularly strong peaks in the shock-motion frequency response that can be directly correlated with a structural frequency. Therefore, it is concluded that the unsteady aerodynamics, at least those represented by the shock motion, would be present in the model despite the structural vibrations encountered during wind-tunnel testing. It should also be noted that given the 8% scale of the wind-tunnel model, any frequency less than 25 Hz would scale to a frequency of less than 2 Hz on the full-scale aircraft. Therefore, there is a significant source of full-scale low-frequency unsteady aerodynamics generated by the shock motion that may not be effectively damped by the flight-control system.

The second significant conclusion reinforced by the shock-motion data is that the shock is not smoothly oscillating across the surface of the wing under a given set of aerodynamic conditions. Rather,

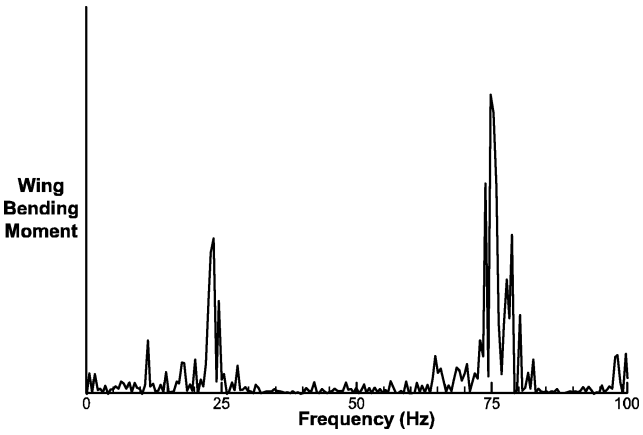

a) Structural dynamics

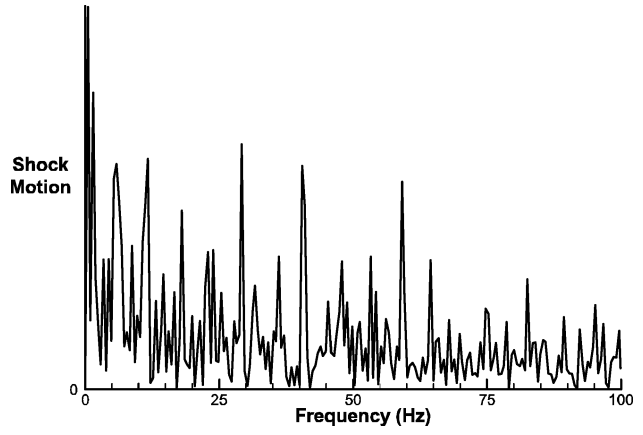

b) Unsteady aerodynamics

Fig. 11 Comparison of model structural-dynamics and unsteady-aerodynamics frequency content; $M = 0.90$, $\alpha = 9.5$ deg.

it tends to stabilize at discrete locations and rapidly transitions between locations. This is illustrated in Fig. 12, which plots the probability of the shock being located at a specific chordwise point on the wing for four angles of attack at Mach 0.9. At 6.5-deg angle of attack the shock is primarily located at 41% chord, with a significantly lower probability that it would be located at 52% chord. In short, under these conditions, the shock motion is limited to approximately 11% of the local wing chord, and it is relatively stable at 41% chord. The probability of the shock being located at positions other than these two locations is small at 6.5-deg angle of attack. At 7.5-deg angle of attack, the shock motion is still confined to two locations, but these locations have moved forward on the wing, now at 33% and 41% chord, and there is less preference for the shock to be located at the forward position than there was at 6.5-deg angle of attack. At 8.5-deg angle of attack a third peak shows up in the probability density function forward of the two peaks identified at the previous angles of attack. The locations where the shock is most likely to be present are now at 26%, 35%, and 42% chord. It is still most likely that the shock will be located at one of the aft two locations, but at this angle of attack, the shock now regularly moves as much as 16% of the wing chord. Finally at 9.5-deg angle of attack there are two primary peaks where the shock resides, 28% and 37% chord, but the shock regularly travels as far back as 43% chord and as far forward as 16% chord. This gives a regularly observed range of shock motion of 27% chord at 9.5-deg angle of attack. The change in aerodynamic load that can be attributed to this range of shock motion is significant, and if this shock motion were to occur asymmetrically on the left and right wings, the rolling moments could be large enough to trigger a lateral event such as wing drop. Forsythe and Woodson[10] demonstrate this type of asymmetric behavior using an unsteady detached-eddy simulation of the full-span F/A-18E aircraft.

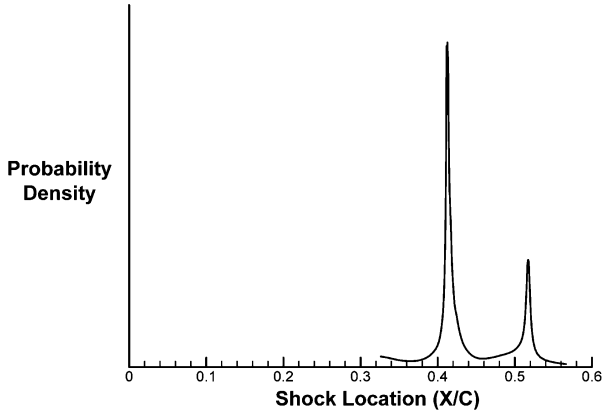

a) $\alpha = 6.5°$

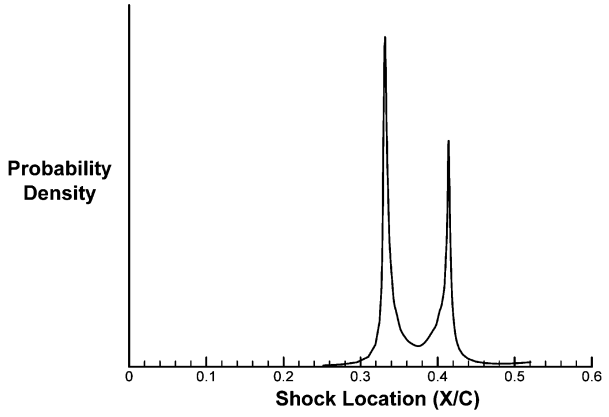

b) $\alpha = 7.5°$

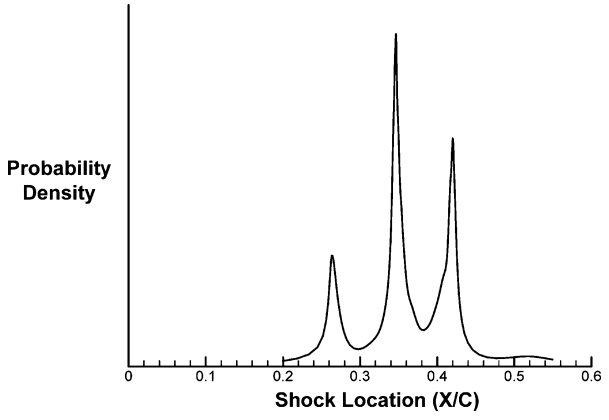

c) $\alpha = 8.5°$

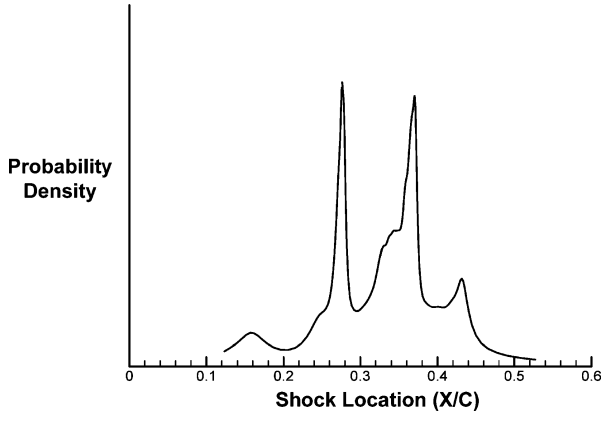

d) $\alpha = 9.5°$

Fig. 12 Probability of the row E shock being located at a given X/C for four angles of attack; $M = 0.90$.

Conclusions

A wind-tunnel test has been conducted measuring a number of unsteady quantities on an 8% scale model of the F/A-18E under conditions where AWS has been encountered on the full-scale aircraft. Among these quantities, the unsteady pressures provide the best insight into the aerodynamic flowfield present on the aircraft under AWS conditions. Accompanying measurements, including outer-wing accelerations, wing-root-bending moments, and load-balance dynamics, were dominated by the structural dynamics of the model/balance/support system. Although useful for general assessment of the unsteadiness of the aerodynamics influencing the model, they cannot be used effectively to investigate the details of the unsteady-flow phenomena present on the aircraft.

The unsteady pressures have been examined both in raw data form and statistically. The raw time histories of the pressures at individual transducer locations clearly showed areas of separated flow as well as extensive shock-wave motion on the wing upper surface. This is particularly true in the vicinity of the leading-edge snag on the F/A-18E, which has been identified as a primary contributor to the lateral instabilities of the aircraft.

Animations, although impossible to show in this paper, and statistical analysis of the chordwise pressure distributions further confirm the large-scale shock motion present on the wing and the angle-of-attack range over which this motion is present. Under AWS conditions, at Mach 0.9 and 9.5-deg angle of attack, shock motion is greatest, with movement in excess of 25% of the local wing chord. Shock excursions of this magnitude typically result in large changes in wing loads. The shock motion on the model also shows significant frequency content below 25 Hz, which scales to less than 2 Hz for the full-scale aircraft. This is significant because the combination of large-scale shock motion and low frequency provides a potential triggering mechanism for lateral instabilities, such as wing drop, which may not be effectively damped by the automatic flight control system.

In general, the structural vibrations of the model do not heavily influence the pressures. More important, the frequency response for the terminal shock on the wing does not correlate with the structural vibration frequencies of the model/balance/sting support system.

Finally, statistical analysis of the shock motion exhibits a bistable and even tristable character of the shock motion and location in the AWS flight regime. The shock does not tend to oscillate smoothly between chordwise locations on the upper surface of the wing but tends to linger at discrete locations, snapping back and forth among them. This characteristic certainly suggests a potential mechanism for a wing-drop event where the right wing may be in one stable shock state while the left wing is in another.

The measurement of unsteady pressures has provided a great deal of diagnostic insight into the complex flow structure present on the F/A-18E wing under AWS conditions. However, the value of unsteady measurements in screening for AWS in a routine testing environment is open for debate. The workforce and hardware resources required to acquire, reduce, and analyze unsteady-pressure data are significant. Without solid techniques and procedures for incorporating unsteady pressures into an AWS screening process, the additional cost of acquiring unsteady-pressure data is likely too high for most programs.

Further research is required into how unsteady pressures might be readily used to screen for AWS. A definite recommendation is that unsteady-pressure transducers should be included on both wings of the aircraft, as opposed to just the single wing in this study. Lateral phenomena could be readily extracted and separated from longitudinal phenomena using time-synchronized pressure data from both wings. This would likely provide entirely new insight into the AWS phenomenon. In addition, the overall coverage of unsteady transducers should be increased over that used in the present study. This would probably require a larger scale model and it would surely require a dynamic data-acquisition system more complex and capable than that used in this analysis.

Acknowledgments

This work was supported by the NASA Aerospace Systems Concepts to Test program, Naval Air Systems Command, and the Office of Naval Research.

References

[1]Traven, R., Hagan, J., and Niewoehner, R., "Solving Wingdrop on the F-18E/F Superhornet," 1998 Rept. to the Aerospace Profession, Society of Experimental Test Pilots, Lancaster, CA, Sept. 1998, pp. 67–84.

[2]Chambers, J., and Hall, R., "Historical Review of Uncommanded Lateral-Directional Motions at Transonic Conditions," AIAA Paper 2003-0590, Jan. 2003.

[3]Hall, R., and Woodson, S., "Introduction to the Abrupt Wing Stall (AWS) Program," AIAA Paper 2003-0589, Jan. 2003.

[4]McMillin, N., Hall, R., and Lamar, J., "Understanding Abrupt Wing Stall with Experimental Methods," AIAA Paper 2003-0591, Jan. 2003.

[5]Mabey, D. G., Welsh, B. L., and Pyne, C. R., "A Review of Rigid Body Response on Sting Supported Models at High Angles of Incidence," *Progress in Aerospace Sciences*, Vol. 28, No. 2, 1991, pp. 133–170.

[6]Woodson, S., Green, B., Chung, J., Grove, D., Parikh, P., and Forsythe, J., "Understanding Abrupt Wing Stall," AIAA Paper 2003-0592, Jan. 2003.

[7]Parikh, P., and Chung, J., "A Computational Study of the AWS Characteristics for Various Fighter Jets, Part I: F/A-18E & F-16C," AIAA Paper 2003-0746, Jan. 2003.

[8]Hwang, C., and Pi, W. S., "Investigation of Steady and Unsteady Pressures Associated with the Transonic Buffeting and Wing Rock of a One-Seventh Scale Model of the F-5A Aircraft," NASA CR 3061, 1978.

[9]Mabey, D. G., "Unsteady Aerodynamics: Retrospect and Prospect," *Aeronautics Journal of the Royal Aeronautical Society*, Review Paper 003, Jan. 1999.

[10]Forsythe, J., and Woodson, S., "Unsteady CFD Calculations of Abrupt Wing Stall Using Detached-Eddy Simulation," AIAA Paper 2003-0594, Jan. 2003.